Available online at www.sciencedirect.com

SciVerse ScienceDirect

journal homepage: www.elsevier.com/locate/he

Destabilization of the $LiNH_2$–LiH hydrogen storage system by aluminum incorporation

L. Fernández Albanesi [a,b], P. Arneodo Larochette [a,b,c], F.C. Gennari [a,b,c,*]

[a] Instituto Balseiro, Universidad Nacional de Cuyo, Argentina
[b] Centro Atómico Bariloche (CNEA), Argentina
[c] Consejo Nacional de Investigaciones Científicas y Técnicas (CONICET), Av. Bustillo 9500, R8402AGP S.C. de Bariloche, Río Negro, Argentina

ARTICLE INFO

Article history:
Received 4 March 2013
Received in revised form
4 June 2013
Accepted 12 July 2013
Available online 8 August 2013

Keywords:
Lithium amide
Ball milling
Halide
Ammonia

ABSTRACT

The lithium amide–lithium hydride system ($LiNH_2$–LiH) is one of the most attractive lightweight materials for hydrogen storage. In an effort to improve its hydrogen sorption kinetics, the effect of 1 mol% $AlCl_3$ addition to $LiNH_2$–LiH system was systematically investigated by differential scanning calorimetry, X-ray diffraction, Fourier transform infrared analysis and hydrogen volumetric measurements. It is shown that Al^{3+} is incorporated into the $LiNH_2$ structure by partial substitution of Li^+ forming a new amide in the Li–Al–N–H system, which is reversible under hydriding/dehydriding cycles. This new substituted amide displays improved hydrogen storage properties with respect to $LiNH_2$–LiH. In fact, a stable hydrogen storage capacity of about 4.5–5.0 wt% is observed under cycling and is completely desorbed in 30 min at 275 °C for the Li–Al–N–H system. Moreover, the concurrent incorporation of Al^{3+} and the presence of LiH are effective for mitigating the ammonia release. The results reveal a common reaction pathway for $LiNH_2$–LiH and $LiNH_2$–LiH plus 1 mol% $AlCl_3$ systems, but the thermodynamic properties are changed by the inclusion of Al^{3+} in the $LiNH_2$ structure. These findings have important implications for tailoring the properties of the Li–N–H system.

1. Introduction

Light metal hydrides or complex hydrides constitute highly desirable materials for hydrogen storage due to their large volumetric hydrogen densities, greater than those obtained in the liquid state, and gravimetric storage densities that exceed DOE targets. Among complex hydrides, the two-component reactive hydride mixture formed from $LiNH_2$ and LiH displays many relevant features. These include reversibility, relatively low operation temperature and low cost. In fact, since the influential paper by Chen et al. in 2002 [1], lithium amide ($LiNH_2$) has been extensively studied as a promising material for hydrogen storage. Hydrogen release occurs in the $LiNH_2$–LiH mixture *via* a reversible solid state decomposition reaction into lithium imide (Li_2NH) and hydrogen:

$$LiNH_2(s) + LiH(s) \leftrightarrow Li_2NH(s) + H_2(g) \quad (1)$$

Reaction (1) theoretical release is 6.5 wt% of hydrogen, with a calculated reaction enthalpy of −44.5 kJ/mol H_2 [1,2].

* *Corresponding author*. Instituto Balseiro (UNCuyo), Centro Atómico Bariloche (CNEA) and Consejo Nacional de Investigaciones Científicas y Técnicas (CONICET), Av. Bustillo 9500, R8402AGP S.C. de Bariloche, Argentina. Tel.: +54 2944 445118; fax: +54 2944 445190.
E-mail address: gennari@cab.cnea.gov.ar (F.C. Gennari).

0360-3199/$ – see front matter
http://dx.doi.org/10.1016/j.ijhydene.2013.07.030

However, further measurements [3,4] have suggested higher values (about −66 kJ/mol H_2) than the previous estimate.

Concerning the mechanism of Reaction (1), Chen et al. have suggested that the dehydriding proceeds *via* direct interaction between solid-phases, which is driven by the exothermic reaction between the positively charged H^+ from $LiNH_2$ and the negatively charged H^- from LiH [1,2]. On the other hand, two independent studies [5,6] have provided strong evidence that Reaction (1) proceeds with the following two elementary reactions ("ammonia mediated mechanism"):

$$2LiNH_2(s) \rightarrow Li_2NH(s) + NH_3(g) \quad (2)$$

$$NH_3(g) + LiH(s) \leftrightarrow LiNH_2(s) + H_2(g) \quad (3)$$

First, $LiNH_2$ decomposes releasing NH_3, which subsequently reacts with LiH to form $LiNH_2$ again and liberates hydrogen. Reaction (3) has shown to be ultrafast and exothermic, leading to full consumption of NH_3 by LiH in the order of microseconds [5,6]. In contrast, using pure $LiNH_2$ as starting material, it has been shown that Reaction (2) is diffusion-controlled and proceeds in minutes [7]. A further study developed by Shaw and co-workers has revealed that the dehydrogenation of the $LiNH_2$–LiH mixture is diffusion-controlled and the rate-limiting step is NH_3 diffusion through the Li_2NH product layer outside the $LiNH_2$ shrinking core [8]. Due to the continued dehydrogenation/hydrogenation cycles, the reaction would involve repeated nucleation of the solid phases and continuous flaking-off of the $LiNH_2$ layer formed at the surface of LiH after reacting with NH_3. An independent investigation has proposed that the dehydrogenation mechanism for Li–N–H takes place through a heterogeneous solid-state reaction controlled by the diffusion of Li^+ and H^- from LiH and $LiNH_2$ with the formation of $Li_2NH_2^+$ as an intermediate state [9]. The results support the hypothesis of a direct solid-state reaction between $LiNH_2$ and LiH, rather than an ammonia-mediated route. The only condition is that the reactants comprise uniformly mixed small particles to ensure direct and frequent contacts. Quite recently, David et al. [10] have proposed a more detailed ion migration model based on the observed non-stoichiometric bulk reaction in the Li_2NH–$LiNH_2$ system, which takes place through the evolution of NH_3. It is suggested that the dehydriding/hydriding performances are highly dependent on the mobility of Li^+ and H^+ ions; dehydrogenation would occur once Li^+ has moved to adjacent vacant tetrahedral sites within the $LiNH_2$ structure creating a Frenkel defect pair. One crucial implication of this mechanism is that an improved hydrogen sorption performance of the Li–N–H system can be expected when increasing the Li^+ mobility by creating a defective structure.

Many attempts have been made to enhance the hydrogen sorption properties of the $LiNH_2$–LiH system, with the main focus on its high desorption temperature and slow reaction kinetics [9,11–17]. Usually three main approaches have been applied to enhance the hydrogen sorption performance of the $LiNH_2$–LiH composite. The first one is the application of ball milling to reduce particle size and facilitate the contact between the reactants [11,12]. The second approach involves the addition of potential catalysts to reduce the desorption temperature [13,17]. The last strategy is focused on the destabilization of the N–H bond by introducing dopants of higher electronegativity than Li [18,19]. Nakamori and Orimo were pioneering in this last approach, where the introduction of a dopant such as Mg provides a route for the synthesis of new families of complex imides/amides and other composite systems [18,19]. A secondary effect of these doped materials might be the introduction of defects in order to maintain charge balance, which could modify the Li^+ mobility.

Some of these approaches were first adopted by Ichikawa et al. [11]. In this initial investigations 1 mol% of Ni, Fe, Co and $TiCl_3$ were added to the $LiNH_2$–LiH system and thermal desorption mass spectroscopy was used to follow the hydrogen desorption behavior. In ball milled mixtures without catalysts, Ichikawa et al. [11,12] observed that ammonia evolution was reduced significantly compared to samples mixed manually. In addition, when the catalysts were added by milling, both NH_3 emission and hydrogen desorption temperature were significantly reduced. The effect was most prominent for $TiCl_3$, where 5.5 wt% of hydrogen was released between 150 and 250 °C, with an activation energy of 110 kJ/mol. Later studies [13] revealed that nanoparticles of Ti or TiO_2 were also effective in reducing the desorption temperature. It was suggested that $TiCl_3$ and TiO_2 react with LiH in the ball milled mixture to produce the corresponding LiCl or Li_2O plus Ti nanoparticles; no activation energies of catalyzed and non-catalyzed materials were reported. These dispersed catalysts were characterized by X-ray absorption spectroscopy [14], indicating that Ti atoms in the titanium compounds have a common chemical bonding. Yao et al. showed that the addition of Mn, V and their oxides to pure $LiNH_2$ reduce its decomposition temperature [15]. However, when these additives are mixed with $LiNH_2$ plus LiH, no discernable effect on the hydrogen desorption kinetics or desorption temperature is observed. From these results, they concluded that the rate-limiting step for dehydrogenation from $LiNH_2$–LiH was the reaction between LiH and NH_3. Matsumoto et al. showed the beneficial effect of milling time on the hydrogen desorption kinetics of the $LiNH_2$–LiH mixture with $TiCl_3$ as catalyst [16]. The activation energy estimated for the Li–N–H system with catalyst was similar to that of Ichikawa et al., but the activation energy of the pristine sample showed a much smaller value of 54 kJ/mol. In a recent work, Isobe et al. analyzed the catalytic role of $TiCl_3$ using X-ray absorption spectroscopy measurements [17]. The results indicate that the Ti atoms in the Ti compounds have a common electronic state, in particular agrees with that of $TiCl_3.5NH_3$. This compound may show catalytic effect in the ammonia mediated reaction, playing a role as a kind of ammonia carrier. Additionally, the kinetics of the Li–N–H system was improved by BN addition [9]. It was suggested that BN improves the mass transport between the two reactants and thus enhances the overall hydrogen desorption kinetics in the heterogeneous solid state reaction between $LiNH_2$ and LiH.

However, from the previous works, it is not clear how titanium (or other catalyst) affects the bulk of the amide catalytically and keeps this role during hydrogen cycling. Motivated by these facts as well as by the ion migration model, we mechanically prepared a $LiNH_2$–LiH composite with 1 mol% $AlCl_3$ addition and investigated their hydrogen storage properties by comparing with $LiNH_2$–LiH. The improved hydrogen sorption properties observed were associated with the

formation of a new amide in the Li–Al–N–H system, where Al^{3+} partially substitutes Li^{+}, generating defects in the $LiNH_2$ structure and modifying the thermodynamics of the system.

2. Experimental

2.1. Synthesis of the composites

The starting materials were commercial $LiNH_2$ (Aldrich, 95%), LiH (Fluka, 95%) and anhydrous $AlCl_3$ (Merck, 98%), which are referred as LN, L and Al, respectively. Due to the high reactivity of the commercial powders with moisture and oxygen, the samples were prepared and manipulated in a MBraun Unilab argon-filled glove box, with oxygen and moisture levels <1 ppm. For all studies, high purity hydrogen (Linde, 99.999%) and argon (Linde, 99.999%) were used.

The sample preparation was carried out by mechanical milling of $LiNH_2$–1.6LiH (LNL) and $LiNH_2$–1.6LiH plus 1 mol% of $AlCl_3$ (LNLAl) mixtures. These composites posses theoretical storage capacities of 5.7 and 5.6 wt% of hydrogen, respectively. The amount of LiH was added in excess with respect to Reaction (1) to avoid, or minimize, the emission of NH_3. Compositions are always expressed in mole. Additionally, a set of mixtures with composition $LiNH_2$–1.6LiH plus X mol% of $AlCl_3$ (with $X = 3$, 5 and 10) were also synthesized for comparison purposes. The mechanical milling was performed in a medium-energy planetary type mill (Fritsch Pulverisette 6) under 0.1 MPa of argon atmosphere. The milling conditions were 400 rpm with a ball mass/sample mass ratio of 40:1. All samples were ball milled for 5 h.

2.2. Characterization of the composites

Structural, textural, thermal and hydrogen storage properties of the composites were studied using powder X-ray diffraction (PXRD, Philips PW 1710/01 Instruments), Fourier transform infrared spectroscopy (FTIR, Perkin Elmer Spectrum 400), N_2 sorption isotherms (Micromeritics ASAP 2020), differential scanning calorimetry (DSC, TA 2910 calorimeter) and a Sieverts-type volumetric equipment.

Structural information of the different samples was obtained by PXRD analysis (CuKα radiation, graphite monochromator) and FTIR analysis. During the PXRD data collection all the samples were maintained under Ar atmosphere using a tightly sealed sample holder to prevent the reaction between samples and air. The gases released during dehydriding of the as-milled mixtures were collected in a degassed quartz optical cell with KBr windows and gas phase spectra at room temperature were taken. For solid-state IR spectroscopy measurements, the selected samples were grounded with dry KBr under purified argon atmosphere and pressed to pellets. Solid-state IR spectra were obtained in the range of 600–4000 cm^{-1} using a specially designed cell. Handling was done inside the glove box to avoid contact with air.

Textural measurements were performed at liquid nitrogen temperature to determine the specific surface area (SSA) based on the Brunauer–Emmett–Teller (BET) method. About 100 mg of sample was evacuated at 150 °C overnight before each measurement. Under this experimental condition no indication of $LiNH_2$ decomposition was observed.

The thermal behavior of the samples was analyzed by DSC using heating ramps between 1 and 25 °C/min and argon flow rate of 122 ml/min. About 5–7 mg of sample was loaded into aluminum capsules hermetically closed in the glove box. The Kissinger method [20] was employed to determine the activation energy of the dehydriding process, according to the following equation:

$$\mathrm{d}\left[\ln\left(\frac{\beta}{T_p^2}\right)\right] \Big/ \mathrm{d}\left(\frac{1}{T_p}\right) = \frac{-E_{app}}{R} \tag{4}$$

where T_p is the peak temperature of the endothermic event, β is the heating rate, E_{app} is the apparent activation energy and R is the ideal gas constant. The slope of the fitted line corresponds to the activation energy (E_{app}) for the reaction.

Pressure–composition isotherms (PCI) and hydrogen sorption kinetics were obtained using a modified Sieverts-type device, coupled with a mass flow controller [21]. The sample is transferred in the glove box into a stainless steel reactor which is then connected to the Sieverts apparatus. Each sample was heated up to the reaction temperature under hydrogen pressure and kept at this temperature for 30 min before hydrogen desorption. First, the sample is dehydrided (first desorption measurement) and consecutively the sample is hydrided (first absorption measurement), both constitute the cycle 1. During the hydrogen desorption, the mass flow controller kept a back pressure almost constant for the entire experiment (0.01 MPa). In a similar way, the hydrogen absorption process was studied using an initial hydrogen pressure of 0.7 MPa, which was kept approximately constant using the mass flow controller. No activation was necessary on the samples. The hydrogen contents reported in the paper are given as weight percent respect to the total mass of the $LiNH_2$–LiH mixture (1:1 mol ratio). The ratio between the theoretical hydrogen storage capacities of 1:1 and 1:1.6 $LiNH_2$–LiH mixtures is 0.88.

3. Results and discussion

In order to analyze the effect of $AlCl_3$ addition on the $LiNH_2$ decomposition, Fig. 1 shows the DSC curves for the as-milled LNL and LNLAl composites. To facilitate the comparison, the DSC curve for the as-received $LiNH_2$ material is also shown. From this figure it can be clearly seen a single endothermic peak around 380 °C corresponding to the melting of $LiNH_2$, which has been reported as due to the release of ammonia gas (curve a) [15,22]. In contrast, the decomposition of LNL and LNLAl composites (curves b and c, respectively) starts at about 180 °C and finishes at different temperatures (385 and 325 °C, respectively). Considering that both samples were milled under the same experimental conditions and the only difference between them is the addition of 1 mol% of $AlCl_3$, the broad DSC peak observed in curve (b) evidences the slower dehydriding rate of the LNL sample. Thermal hydrogen desorption curves combined with gas FTIR analyses allow to determine that hydrogen is the main gas released from 180 to 325 °C for the LNL and LNLAl composites. Simultaneously,

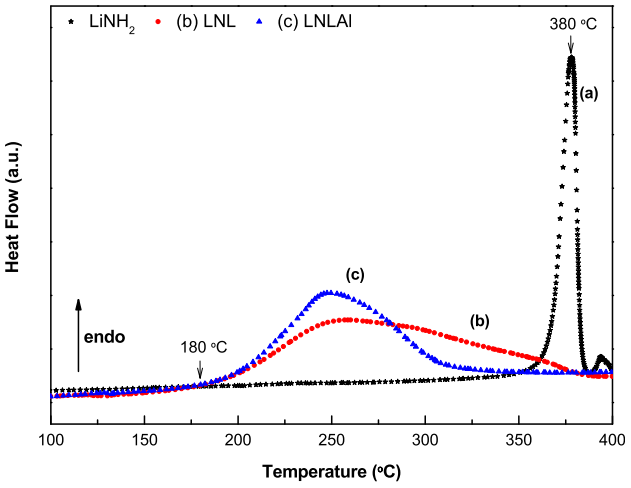

Fig. 1 – DSC curves of (a) as-purchased $LiNH_2$; (b) as-milled LNL; (c) as-milled LNLAl. Heating ramp of 5 °C/min.

minor amounts of NH_3 are detected during LNL decomposition from 280 °C (in the order of 500 ppm), which increase at 300 °C (1300 ppm) (see Figs. S1 and S2, Supplementary Material). This result is in agreement with previous studies, where NH_3 was identified using thermal desorption mass spectroscopy [11]. On the contrary, no NH_3 emission is detected from the decomposition of LNLAl sample up to 350 °C, using gas-FTIR technique. FTIR analyses suggest that $AlCl_3$ would enhance the solid–gas reaction between LiH and NH_3. Therefore, the more pronounced endothermic peak obtained from 180 to 325 °C for the composite containing 1 mol% of $AlCl_3$ evidences that the additive improves the hydrogen desorption kinetics and avoids NH_3 emission.

Fig. 2 compares the hydrogen absorption (Fig. 2A) and desorption (Fig. 2B) kinetics of LNL and LNLAl samples at 300 °C. Both composites show similar sorption behavior, with a subtle faster hydrogen sorption rate for the LNLAl composite and a total hydrogen storage about 5.0 wt%. In particular, hydrogen sorption behavior of the LNL composite slightly improves during hydrogen cycling at 300 °C. In samples of the same batch, we performed only one hydrogen cycle after keeping them at 300 °C for at least 12 h and observed analogous sorption rates. Then, we could associate this effect on the sorption kinetics with the thermal treatment of the sample. In contrast, the system containing Al is stable after the first cycle. The main difference between both composites is observed during dehydriding cycling. Practically complete dehydriding of LNLAl sample (>4.5 wt% of hydrogen) occurs in 20 min, while for LNL composite dehydriding continues asymptotically and is uncompleted after 60 min. Additional hydrogen absorption/desorption cycling of the LNLAl composite up to seven cycles demonstrates that the material is stable, keeping both the hydrogen storage capacity as well as the hydrogen absorption/desorption rate during cycling (Fig. 3). No clear degradation is detectable and the differences in the hydrogen storage between cycles are associated with uncompleted desorption (as it will be shown from FTIR measurements). The small steps observed in the desorption curves are produced by the opening of the mass flow controller, in

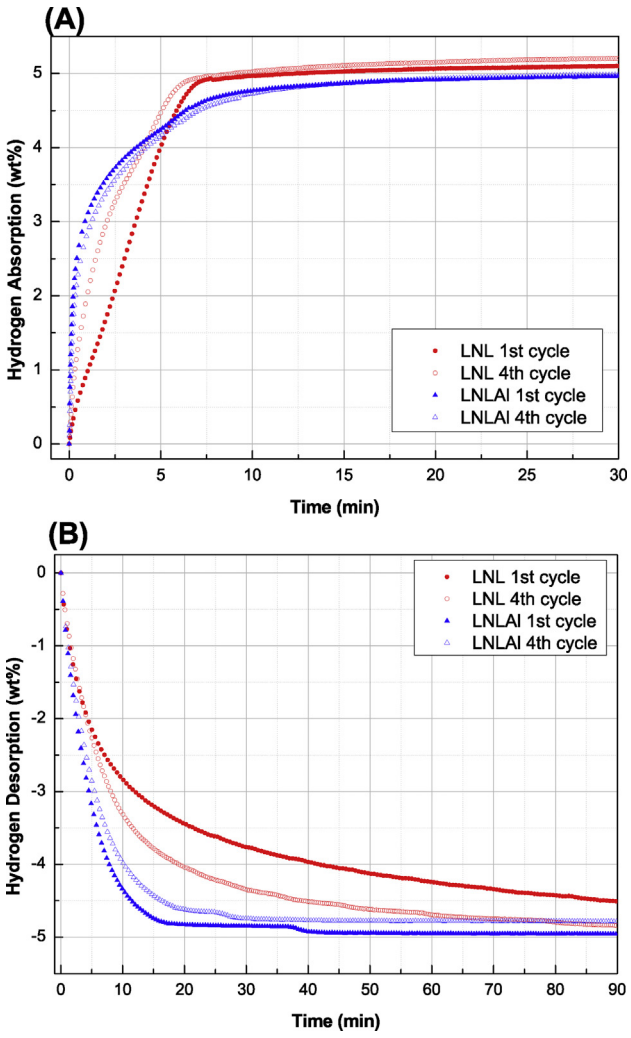

Fig. 2 – Hydrogen sorption curves for LNL and LNLAl composites at 300 °C after first and fourth cycle. (A) Absorption under 0.7 MPa of hydrogen pressure; (B) Desorption at 0.01 MPa of hydrogen pressure.

order to keep the pressure almost constant. These small perturbations do not significantly affect the measurement process.

The differences between the hydrogen storage properties of LNL and LNLAl composites are enhanced at 275 °C (Fig. 4). Clearly, the LNL sample deteriorates during hydrogen absorption/desorption cycling, with a reduction of both the sorption rate and hydrogen storage capacity. In contrast, the addition of only 1 mol% of $AlCl_3$ strongly modifies the sorption rate and the hydrogen storage capacity, which are relatively constant during four cycles for the LNLAl composite. Appropriate hydrogen storage reversibility was also observed after three cycles for a $LiNH_2$–LiH–0.1 $TiCl_3$ composite, but the measurements were performed under non-isothermal conditions up to 400 °C [12]. On the other hand, the best results on hydrogen cycling were obtained by Osborn et al. [23]. They showed long-term cyclic durability of a nano-engineered $LiNH_2$–LiH system at 285 °C. A small decrease in the kinetics of dehydrogenation conducted to a 10% reduction in the

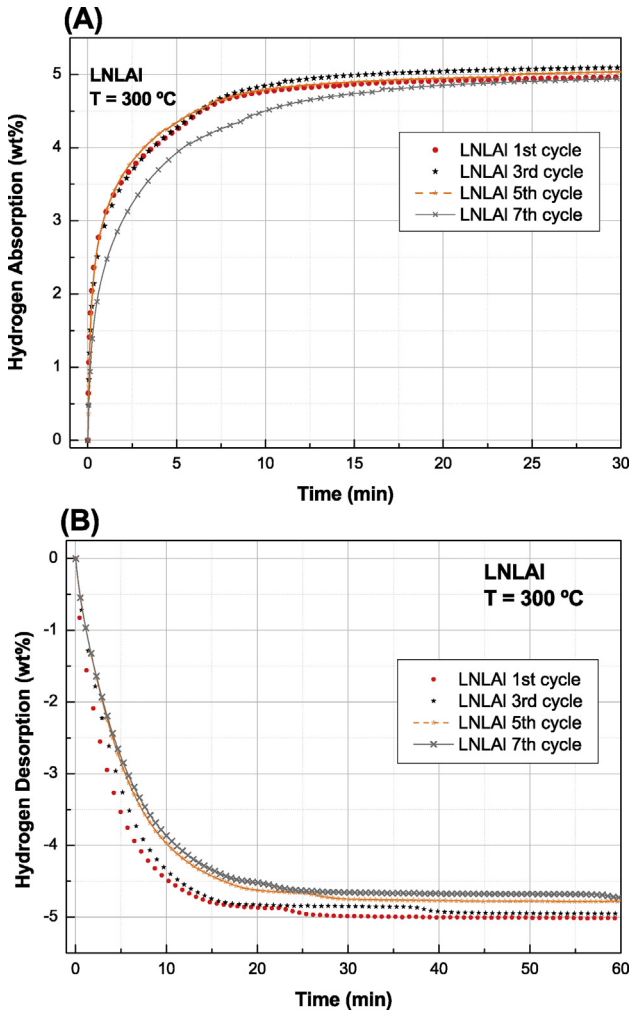

Fig. 3 – Hydrogen sorption cycling for the LNLAl composite at 300 °C. (A) Absorption under 0.7 MPa of hydrogen pressure; (B) Desorption at 0.01 MPa of hydrogen pressure.

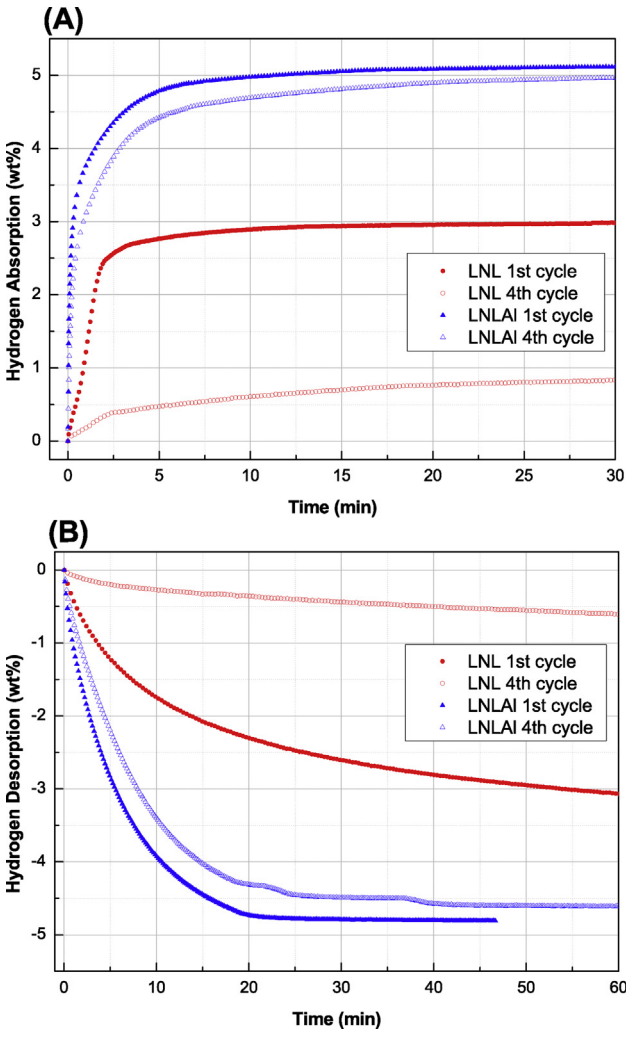

Fig. 4 – Hydrogen sorption curves for LNL and LNLAl composites at 275 °C after first and fourth cycle. (A) Absorption under 0.7 MPa of hydrogen pressure; (B) Desorption at 0.01 MPa of hydrogen pressure.

amount of hydrogen liberated during 2.5 h of hydrogen desorption. Good hydriding/dehydriding stability and superior dehydriding kinetics was obtained for the LNLAl composite, in comparison with previous works [12,23] and with the LNL composite. During these absorption/desorption cycles, it is assumed that the main desorbed gas is hydrogen, but we cannot totally exclude the presence of minor amounts of ammonia, particularly because desorption in the volumetric equipment is conduced under dynamic vacuum conditions. In this way, the NH_3 produced by Reaction (2) may not keep a sufficiently long contact with LiH to form hydrogen [24]. Nevertheless, gas FTIR analyses during dehydriding process do not detect the presence of NH_3.

Considering that both LNL and LNLAl composites were synthesized using the same experimental conditions, the only difference was the addition of 1 mol% of $AlCl_3$. To clarify if the presence of $AlCl_3$ introduces structural/microstructural modifications, both PXRD and SSA studies were performed. Fig. 5A and B shows the PXRD profiles of the LNL and LNLAl composites, respectively, after milling for 5 h and re-hydriding at 300 °C. As-milled samples show broad diffraction peaks, which suggest small size of the crystallites and/or lattice distortions. The crystallite size for $LiNH_2$ determined by the Scherrer equation is in the nanometer range for both composites (about 14–15 nm). No diffraction peaks from $AlCl_3$ or other newly formed phases are detected. In particular, the LiCl formation was not verified because the main diffraction peaks were close to the peak position of $LiNH_2$, as was mentioned in a previous study on an as-milled $LiNH_2$–metal chloride system [25]. After thermal desorption, the diffraction peaks of the imide and LiH are clearly identified (PXRD pattern not shown). These results demonstrate that the dehydrogenation treatments lead to the conversion of $LiNH_2$ into Li_2NH. During rehydriding, $LiNH_2$ is formed from imide both in LNL and LNLAl samples, with a crystallite size of ~35 nm. The inspection of the specific surface area by BET method provides the same value of 24 m^2/g for as-milled LNL and LNLAl samples. This indicates that a differential reactivity due to SSA is not expected. Therefore, although $AlCl_3$ would assist the

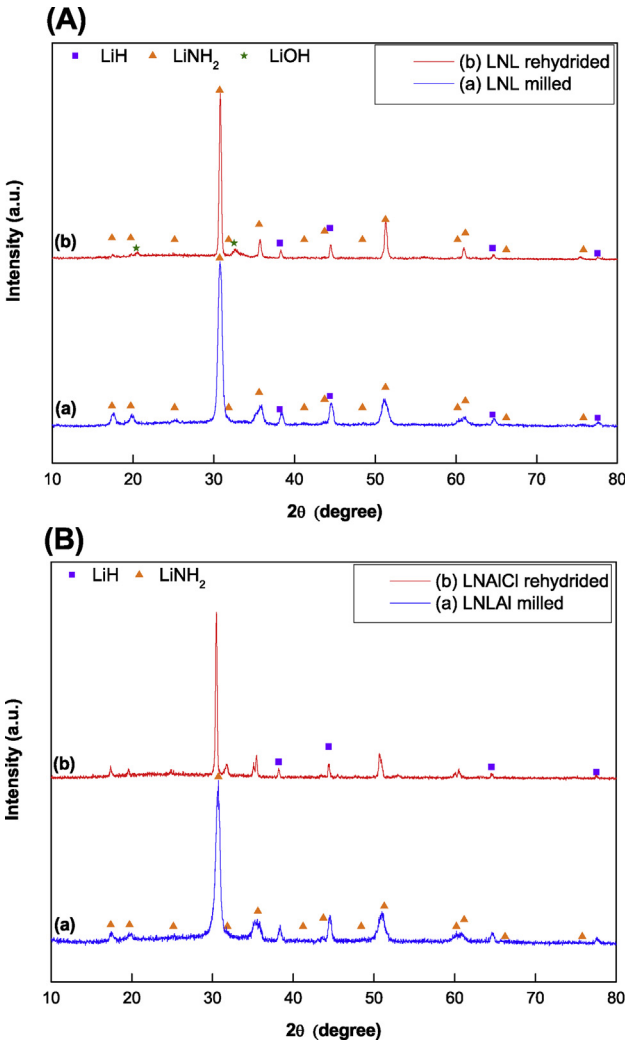

Fig. 5 – X-ray diffraction patterns of (A) LNL and (B) LNLAl composites. (a) after milling; (b) after first rehydriding cycle. Hydrogen sorption cycles performed at 300 °C.

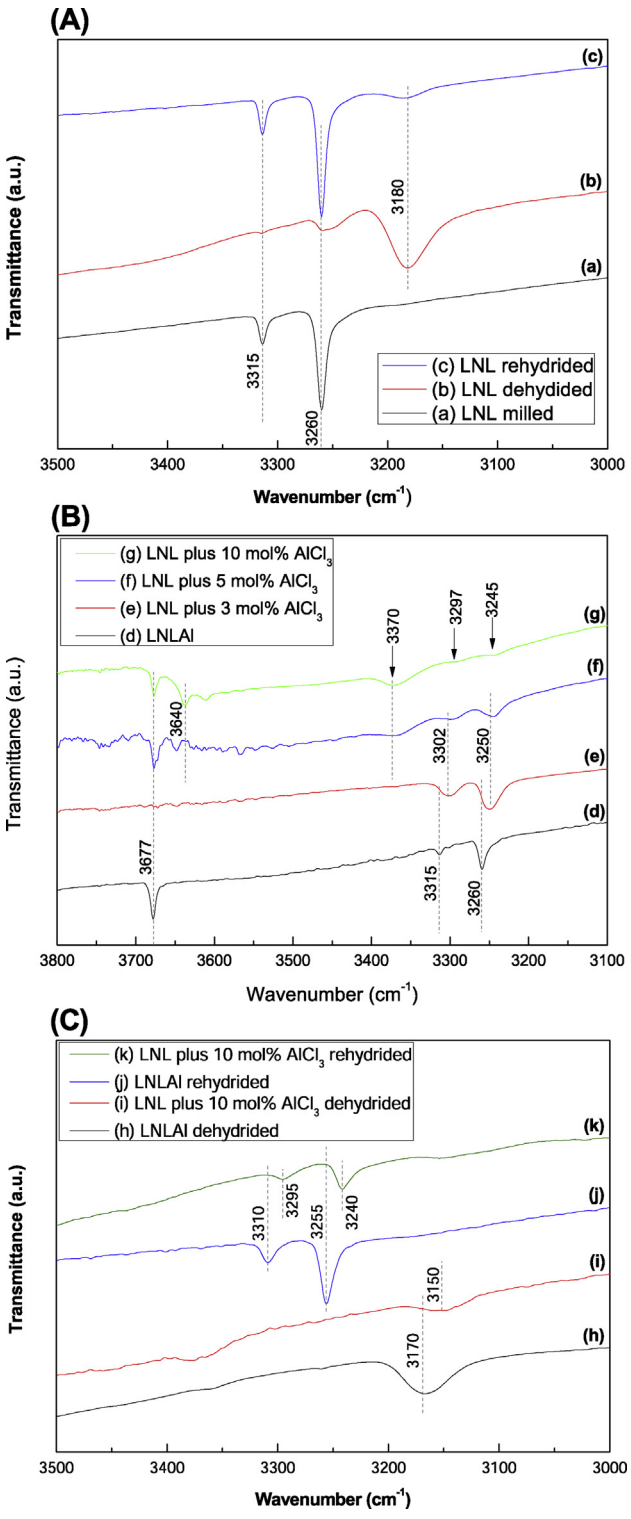

Fig. 6 – FTIR spectra of the: (A) LNL composite; (B) as-milled LNLAl composite with different $AlCl_3$ content; (C) LNLAl composite. (a) as-milled LNL; (b) after dehydriding; (c) after rehydriding; (d, e, f, g) as-milled LNLAl composite with 1, 3, 5 and 10 mol% of $AlCl_3$, respectively; (h, i) after dehydriding of LNLAl with 1 and 10 mol%, respectively; (j, k) after rehydriding of LNLAl with 1 and 10 mol%, respectively.

refinement of $LiNH_2$ and LiH during milling increasing the number of interfaces between them, both crystallite size and SSA values do not support this assumption.

To obtain additional structural information about the interaction between $AlCl_3$ and $LiNH_2$–LiH after milling and hydrogen absorption/desorption cycles, investigations were made by infrared spectroscopy. Fig. 6A (curves a–c) shows FTIR spectra for the LNL composite after milling, dehydriding and rehydriding, respectively. For comparison, FTIR spectra of LNL after milling with different amounts of $AlCl_3$ (1, 3, 5 and 10 mol%) are included (Fig. 6B, curves d–g) as well as those after rehydrogenation/dehydrogenation for the samples with 1 mol% and 10 mol% of $AlCl_3$ (Fig. 6C, curves h–k). In the as-milled and rehydrided LNL composite, $LiNH_2$ displays two main peaks at 3315 and 3260 cm^{-1}, corresponding to asymmetric and symmetric stretching of N–H bonds in the $LiNH_2$ molecule, respectively (Fig. 6A, curves a and c) [3]. Some interesting features are observed from FTIR spectra of the as-milled LNL samples with different mol% of $AlCl_3$ (Fig. 6B): those bands in the LNL composite (3315 and 3260 cm^{-1}) shift

progressively to smaller wave numbers by $AlCl_3$ addition (with 10 mol% of $AlCl_3$: N–H asymmetric vibration, 3297 cm^{-1}; N–H symmetric vibration, 3245 cm^{-1}). These IR bands cannot be easily assigned as corresponding to Li and/or Al amide/imides reported in the literature. Similar bands were previously observed after 48 h of milling of the $LiAl(NH_2)_4$:4LiH mixture [26] as well as after 24 h of milling of the Li_2AlH_6–1$LiNH_2$ mixture [27]. In particular, Janot et al. [26] suggested that these bands are associated with a new ternary Li–Al amide formed during milling, which can be responsible of the thermodynamic change of the system. As an interesting result, the bands at 3297 and 3245 cm^{-1} are also identified in the rehydrided LNLAl material (Fig. 6C, curves k and j), which appears shifted at 3295 and 3240 cm^{-1} and constitutes an evidence of the reversibility of the new ternary Li–Al amide. It is apparent that during hydrogen cycling, an arrangement of the Li–Al–N–H structure has occurred with respect to the as-milled samples, as can be deduced from the slight shift of these bands (compare Fig. 6B, curves d and g, with Fig. 6C, curves j and k).

On the other hand, it can be seen from Fig. 6B that as the $AlCl_3$ content increases from 1 to 10 mol%, two extra bands at 3370 and 3640–3650 cm^{-1} are also discernible (curve f and g). For the 10 mol% of $AlCl_3$, the broad peaks at 3370 and 3640 cm^{-1} are the prevailing ones in the spectrum, whereas the bands at 3290 and 3240 cm^{-1} of the ternary amide can also be recognized. These last bands detected for as-milled LNL composites with 5 and 10 mol% of $AlCl_3$ (Fig. 6B, curves f and g) disappear after rehydriding (Fig. 6C, curve j). Then, the experimental evidence suggests the formation of a minority phase with different structure from those of the starting materials and the new Li–Al amide, which is not reversible. In addition, in some samples the band at 3677 cm^{-1} characteristic of the LiOH presence is detected, possibly due to the interaction of the powders with moisture during handling and/or to the KBr windows of the FTIR cell [28].

In the desorbed LNL sample, Li_2NH shows two peaks at 3180 and 3250 cm^{-1} (Fig. 6A, curve b), as reported previously [3,25]. As stated for PXRD, this result demonstrates the conversion of $LiNH_2$ into Li_2NH during dehydriding/hydriding cycling. Additionally, the band at 3260 cm^{-1} associated with the symmetric stretching of N–H bonds in the $LiNH_2$ molecules are observed, as evidence of the uncompleted desorption. After dehydriding, the systems containing 1 and 10% of $AlCl_3$ display the same stretch at 3170 cm^{-1} and 3150 cm^{-1}, respectively, which is due to the presence of the N–H bond. Then, both amide and imide bands in the Li–Al–N–H system appear shifted respect to the Li–N–H, in a similar way to previous observations [26,27]. The shifts observed in the FTIR spectra for the Li–Al–N–H system can be understood by considering that $LiNH_2$ and $AlCl_3$ reacts during milling forming a substituted amide and LiCl. At the present, we are performing nuclear magnetic resonance measurements to gain insight into this new amide structure.

The incorporation of the Al^{3+} into the $LiNH_2$ lattice induces two effects: it generates Li^+ vacancies in order to maintain charge balance and modifies the interaction between the cation and NH_2^- (Li^+ and Al^{3+} have different charge and electronegativity). To clarify if the incorporation of Al^{3+} (1 mol%) in the amide structure modifies the thermodynamic properties of the system, pressure composition isotherms (PCI) were performed after about two–three cycles of hydriding/dehydriding. Fig. 7A and B shows typical PCI curves at 300 °C and 275 °C obtained over a period of 12 h and each data point equilibrated for approximately 15 min. The hydrogen pressure increases (decreases) monotonically with the amount of hydrogen absorbed (desorbed), with the consequent absence of a well-defined plateau. Only for the LNL composite during absorption a plateau could roughly be identified. The hydrogen storage capacity and the onset equilibrium pressure for desorption at each temperature are higher for the Li–Al–N–H system. In particular, the onset equilibrium hydrogen desorption pressures are 0.28 MPa (0.12 MPa) and 0.48 MPa (0.25 MPa) for LNL and LNLAl at 300 °C (275 °C), respectively (Fig. 7). Then, the addition of only 1 mol% of $AlCl_3$ modifies the thermodynamics of the system. Additionally, at the beginning of desorption reaction the higher onset equilibrium hydrogen pressure for LNLAl would produce a higher driving force. Assuming that the Al^{3+} was incorporated in the $LiNH_2$ structure, the more covalent interaction of Al^{3+} with NH_2^- compared to Li^+ with NH_2^-, can contribute to the thermodynamic destabilization of the $LiNH_2$–LiH system. Our results are in accordance with a recent

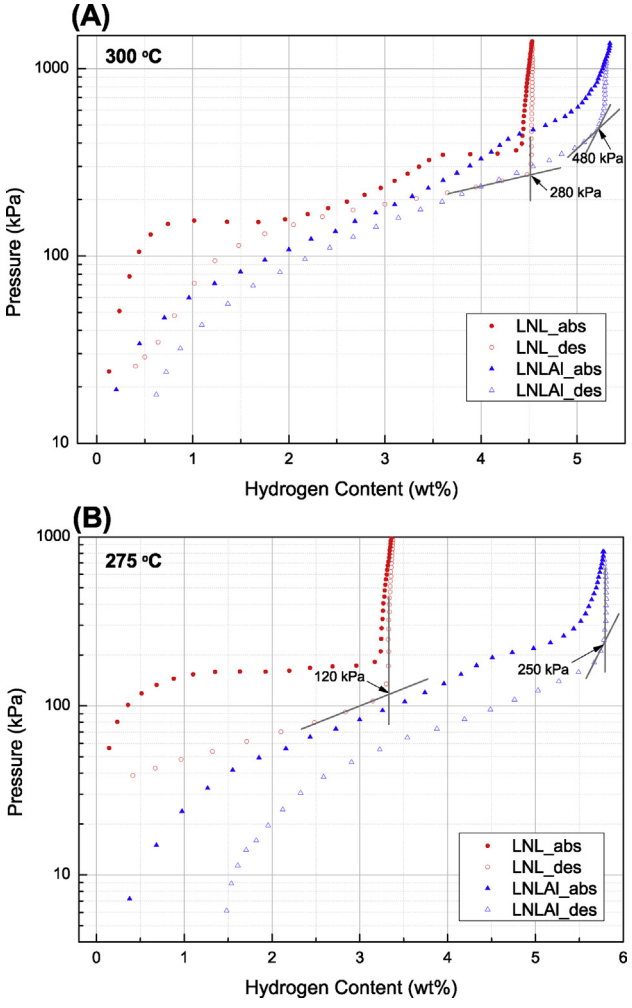

Fig. 7 – Pressure–composition isotherms (PCI) of LNL and LNLAl composites at: (A) 300 °C and (B) 275 °C.

study on the polarizing effects of the metallic cations and the force constants of the N–H covalent bonds of the amides [29].

In order to compare with previous studies [6,16] where different additives were added to the $LiNH_2$–LiH system, the activation energy was determined using the Kissinger method (Eq. (4)). Fig. 8 shows the corresponding Kissinger plot for the LNL and LNLAl composites. The DSC curves measured to construct Fig. 8 showed high sensitivity to different experimental variables, such as the closing procedure of the aluminum capsules. For this reason, under standardizing conditions, several measurements were performed at each heating ramp and the average peak temperature is displayed in the figure. There is a considerably spread of the measured data, which results in large error bars, as can be seen in the Figure. Additionally, data points do not clearly lie on a straight line as expected from the Kissinger plot, even though the range of used heating ramps is relatively small (1–25 °C/min) due to experimental constraints. However, in order to compare with reported results, the apparent activation energies were calculated with the widely used Kissinger method. The activation energies obtained are 113 ± 5 kJ/mol and 109 ± 3 kJ/mol (correlation coefficient $R = 0.972$ and 0.998), for the LNL and LNLAl composites, respectively. These activation energies values are similar and in the same order of magnitude to the previously reported [6,7,16,24]. Pinkerton determined an activation energy of 127 ± 13 to 131 ± 11 kJ/mol for the direct decomposition of ball milled $LiNH_2$ [24]. Markmaitree et al. [7] found that the activation energy for the decomposition of $LiNH_2$ without ball milling was 246 kJ/mol, which was reduced to138 kJ/mol after ball milling for 3 h. Ichikawa et al. [6] have reported a value of 110 kJ/mol for activation energy during hydrogen desorption from $LiNH_2$–LiH catalyzed by 1 mol% of $TiCl_3$ system. However, they were not able to determine the activation energy for the non-catalyzed mixture. On the other hand, Matsumoto et al. [16] calculated an activation energy of 95 kJ/mol for Ti^{3+} doped $LiNH_2$–LiH. They suggested that Ti^{3+} species do not act as a chemical catalyst, but enhance the reaction rate *via* a different role. All reported values of activation energy for as-milled $LiNH_2$ [7,22], $LiNH_2$–LiH and $LiNH_2$–LiH with additive [6,16] are close to the activation energies determined in the present work. This finding suggests that $AlCl_3$ does not play a catalytic role during desorption.

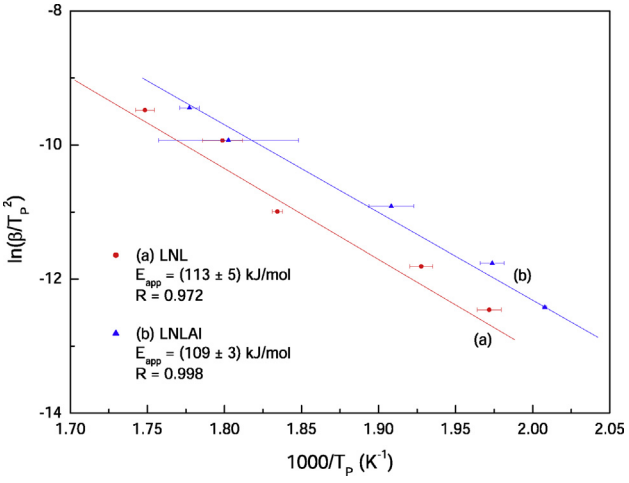

Fig. 8 – Kissinger plot for LNL and LNLAl composites. The hydrogen desorption temperatures were obtained from DSC curves using heating ramps between 1 and 25 °C/min.

Finally, it can be concluded that the incorporation of Al^{3+} into the $LiNH_2$ structure has three consequences. The first one is the modification of the thermodynamic behavior of the Li–N–H system. A recent work studied the promotion of the covalent character of the metal–nitrogen bond by the formation of amides with more electronegative metals than Li [29]. It was shown that Al^{3+} is more effective than other metallic cations (K, Na, Li, Ba, Sr, Mg) to create an electric field and thus to deform the electronic cloud of the NH_2^-, modifying the N–H bond force constant. Our result confirms this tendency and the destabilization of the N–H bonds by Al^{3+} was demonstrated by thermodynamics measurements. The second consequence of the Al^{3+} incorporation is its effect on the hydrogen sorption kinetics and the hydrogen storage capacity. A previous work demonstrated that the structural relationship between $LiNH_2$ and Li_2NH allows a topotactic de/rehydrogenation *via* a solid solution form $Li_{(1+x)}NH_{(2-x)}$ [10]. In this model, $LiNH_2/Li_2NH$ decomposition and hydrogenation processes (Reaction (1)) are dependent on the migration of Li^+ and H^+ ions. Considering the ability of these structures to accommodate large numbers of cation defects [30], if all Al from 1 mol% of $AlCl_3$ is incorporated in the $LiNH_2$ structure, the formation of about 5% Li vacancies is possible. The close structural relationship between $LiNH_2$ and Li_2NH raises the possibility to form vacancy ordering/disordering in Li–Al–N–H hydrided state and the formation of Frenkel defects in the dehydrided state. Then, Al^{3+} improves the sorption kinetics and the hydrogen storage capacity by increasing Li^+ mobility and/or disorder in the $LiNH_2$ structure. Additionally, the inclusion of Al^{3+} into the $LiNH_2$ structure avoids the NH_3 releasing. In the Li–N–H system with $TiCl_3$ or LiCl additives, formation of ammoniate $TiCl_3.5NH_3$ [17] or amide–halide $Li_4(NH_2)_3Cl$ [31], respectively, have been proposed as mitigating the NH_3 release. In the present case, although the formation of ammoniate species can not be ruled out, the precise operating mechanism is unknown. Our proposal is that the improved lithium mobility due to the introduction of vacancies in the amide structure favors the topotactic transformation from $LiNH_2$ to Li_2NH for hydrogen desorption, thus reducing the emission of NH_3.

In this context, the same value of activation energy obtained for both LNL and LNLAl samples during dehydriding could be discussed (Fig. 8). A change in the activation energy is typically related to a change in the reaction mechanism or in the energy state of the reactant(s). We propose that the incorporation of Al^{3+} into the $LiNH_2$ lattice generates high-density of defects and increases the energy state of $LiNH_2$ (reactant), but also the energy state of Li_2NH (product). FTIR studies demonstrate that Al^{3+} remains incorporated during hydrogen cycling in both the hydrided ($LiNH_2$) and dehydrided (Li_2NH) states (Fig. 6). Then, considering that the energy states of the reactant and the product were modified and the activation energy values remain constant, the role of the additive is not catalytic. Therefore, the introduction of Al^{3+} in the $LiNH_2$ lattice, with the consequent creation of defects and increment

of the disorder, enhances the reaction rate (Figs. 1–4) and modifies the thermodynamic behavior of the system (Fig. 7).

4. Conclusions

In this work, hydrogen sorption properties of $LiNH_2$–LiH plus 1 mol% of $AlCl_3$ were analyzed and compared with $LiNH_2$–LiH. An improvement in the rehydriding and dehydriding rates, hydrogen storage capacities and stability under hydrogen cycling was observed for the LNLAl composite. In addition, no ammonia was noticed in the detection limit of the gas FTIR, indicating that the addition of $AlCl_3$ aided the suppression of ammonia release and the good cycling stability. PXRD and SSA measurements show that $AlCl_3$ does not assist the refinement of the $LiNH_2$–LiH mixture during milling. In fact, FTIR studies of rehydrided/dehydrided products allowed determining the formation of a Li–Al–N–H amide after milling, which is reversible during hydrogen cycling, and also the formation of a minority phase, which does not remain during hydrogen cycling. The new Li–Al–N–H amide was characterized by the shift of the asymmetric and symmetric stretching of N–H bonds with respect to $LiNH_2$, which is indicative of different NH_2^- environment due to the Al^{3+} incorporation. In a similar way, in the dehydrided state of the Li–Al–N–H system, a shift of the symmetric stretching of the N–H bond with respect to Li_2NH was identified. It was demonstrated that the inclusion of Al^{3+} into the $LiNH_2$ structure modifies the thermodynamic properties of the $LiNH_2$–LiH system, which is the main responsible in improving the hydrogen sorption behavior. No catalytic role of Al-containing additive was revealed. Current work is targeted towards the clarification of intermediate phases during hydriding/dehydriding by NMR measurements.

Acknowledgment

This study has been partially supported by CONICET (National Council of Scientific and Technological Research), CNEA (National Commission of Atomic Energy), ANPCyT (PICT N° 1049) and Instituto Balseiro (University of Cuyo).

Appendix A. Supplementary data

Supplementary data related to this article can be found at http://dx.doi.org/10.1016/j.ijhydene.2013.07.030.

REFERENCES

[1] Chen P, Xiong Z, Luo J, Lin J, Tan LT. Interaction of hydrogen with metal nitrides and imides. Nature 2002;420–421:302–4.
[2] Chen P, Xiong Z, Luo J, Lin J, Tan LT. Interaction between lithium amide and lithium hydride. J Phys Chem B 2003;107:10967–70.
[3] Kojima Y, Kawai Y. IR characterizations of lithium imide and amide. J Alloys Compd 2005;395:236–9.
[4] Isobe S, Ichikawa T, Tokoyoda K, Hanada N, Leng H, Fujii H, et al. Evaluation of enthalpy change due to hydrogen desorption for lithium amide/imide system by differential scanning calorimetry. Thermochim Acta 2008;468:35–8.
[5] Hu YH, Ruckenstein E. Ultrafast reaction between LiH and NH_3 during H_2 storage in Li_3N. J Phys Chem A 2003;107:9737–9.
[6] Ichikawa T, Hanada N, Isobe S, Leng H, Fujii H. Mechanism of novel reaction from $LiNH_2$ and LiH to Li_2NH and H_2 as a promising hydrogen storage system. J Phys Chem B 2004;108:7887–92.
[7] Markmaitree T, Ren R, Shaw LL. Enhancement of lithium amide to lithium imide transition via mechanical activation. J Phys Chem B 2006;110:20710–8.
[8] Shaw LL, Osborn W, Markmaitree T, Wan X. The reaction pathway and rate-limiting step of dehydrogenation of the $LiNH_2$ + LiH mixture. J Power Sources 2008;177:500–5.
[9] Aguey-Zinsou KF, Yao J, Guo ZX. Reaction paths between $LiNH_2$ and LiH with effects of nitrides. J Phys Chem B 2007;111:12531–6.
[10] David WIF, Jones MO, Gregory DH, Jewell CM, Johnson SR, Walton A, et al. A mechanism for non-stoichiometry in the lithium amide/lithium imide hydrogen storage reaction. J Am Chem Soc 2007;129:1594–601.
[11] Ichikawa T, Isobe S, Hanada N, Fujii H. Lithium nitride for reversible hydrogen storage. J Alloys Compd 2004;365:271–6.
[12] Ichikawa T, Hanada N, Isobe S, Leng HY, Fujii H. Hydrogen storage properties in Ti catalyzed Li-N-H system. J Alloys Compd 2005;404–406:435–8.
[13] Isobe S, Ichikawa T, Hanada N, Leng HY, Fichtner M, Fuhr O, et al. Effect of Ti catalyst with different chemical form on Li-N-H hydrogen storage properties. J Alloys Compd 2005;404–406:439–42.
[14] Isobe S, Ichikawa T, Kojima Y, Fujii H. Characterization of titanium based catalyst in the Li-N-H hydrogen storage system by X-ray absorption spectroscopy. J Alloys Compd 2007;446–447:360–2.
[15] Yao JH, Shang C, Aguey-Zinsou KF, Guo ZX. Desorption characteristics of mechanically and chemically modified $LiNH_2$ and ($LiNH_2$ + LiH). J Alloys Compd 2007;432:277–82.
[16] Matsumoto M, Haga T, Kawai Y, Kojima Y. Hydrogen desorption reactions of Li-N-H hydrogen storage system: estimation of activation free energy. J Alloys Compd 2007;439:358–62.
[17] Isobe S, Hino S, Ichikawa T, Kojima Y. Identifying catalyst in Li-N-H system by x-ray absorption spectroscopy. Appl Phys Lett 2011;99:013101.
[18] Nakamori I, Orimo S. Li-N based hydrogen storage materials. Mater Sci Eng B 2004;108:48–50.
[19] Nakamori I, Orimo S. Destabilization of Li-based complex hydrides. J Alloys Compd 2004;370:271–5.
[20] Kissinger HE. Reaction kinetics in differential thermal analysis. Anal Chem 1957;29:1702–6.
[21] Meyer G, Rodríguez DS, Castro F, Fernández G. Automatic device for precise characterization of hydride forming materials. Hydrogen Energy Prog XI 1996;2:1293–8.
[22] Varin RA, Jang M, Polanski M. The effects of ball milling and molar ratio of LiH on the hydrogen storage properties of nanocrystalline lithium amide and lithium hydride ($LiNH_2$ + LiH) system. J Alloys Compd 2010;491:658–67.
[23] Osborn W, Markmaitree T, Shaw LL. The long-term hydriding and dehydriding stability of the nanoscale $LiNH_2$ + LiH hydrogen storage system. Nanotechnology 2009;20:204028.
[24] Pinkerton FE. Decomposition kinetics of lithium amide for hydrogen storage materials. J Alloys Compd 2005;400:76–82.
[25] Miyaoca H, Fujii H, Yamamoto H, Hino S, Nakanishi H, Ichiawa T, et al. Improvement of reaction kinetics by metal

chloride on ammonia and lithium hydride system. Int J Hydrogen Energy 2012;37:16025–30.
[26] Janot R, Eymery JB, Tarascon JM. Decomposition of $LiAl(NH_2)_4$ and reaction with LiH for a possible reversible hydrogen storage. J Phys Chem C 2007;111:2335–40.
[27] Kojima Y, Matsumoto M, Kawai Y, Haga T, Ohba N, Miwa K, et al. Hydrogen absorption and desorption by the Li-Al-N-H system. J Phys Chem B 2006;110:9632–6.
[28] Tanaka S, Taniguchi M, Nakatani M, Yamaki D, Yamawaki M. In situ observation of surface –OH and –OD on lithium oxide. J Nucl Mater 1995;218:335–8.
[29] Eymery JB, Truflandier L, Charpentier T, Chotard JN, Tarascon JM, Janot R. Studies of covalent amides for hydrogen storage systems: structures and bonding of the $MaI(NH_2)_4$ phases with M = Li, Na and K. J Alloys Compd 2010;503:194–203.
[30] Wu H. Structure of ternary imide $Li_2Ca(NH)_2$ and hydrogen storage mechanisms in amide-hydride system. J Am Chem Soc 2008;130:6515–22.
[31] Anderson AA, Chater PA, Hewett DR, Slater PR. Hydrogen storage and ionic mobility in amide-halide systems. Faraday Discuss 2011;151:271–84.